Darcy's Law without Friction in Active Nematic Rheology

Fraser Mackay,[1] John Toner,[2] Alexander Morozov,[1] and Davide Marenduzzo[1]
[1]*SUPA, School of Physics and Astronomy, University of Edinburgh, Peter Guthrie Tait Road, Edinburgh EH9 3FD, United Kingdom*
[2]*Institute for Fundamental Science and Department of Physics, University of Oregon, Eugene, Oregon 97403, USA*

(Received 18 September 2019; revised manuscript received 19 February 2020; accepted 24 March 2020; published 4 May 2020)

We study the dynamics of a contractile active nematic fluid subjected to a Poiseuille flow. In a quasi-1D geometry, we find that the linear rheology of this material is reminiscent of Darcy's law in complex fluids, with a pluglike flow decaying to zero over a well-defined "permeation" length. As a result, the viscosity increases with size, but never diverges, thereby evading the yield stress predicted by previous theories. We find strong shear thinning controlled by an active Ericksen number quantifying the ratio between external pressure difference and internal active stresses. In 2D, the increase of linear regime viscosity with size only persists up to a critical length beyond which we observe active turbulent patterns, with very low apparent viscosity. The ratio between the critical and permeation length determining the stability of the Darcy regime can be made indefinitely large by varying the flow aligning parameter or magnitude of nematic order.

DOI: 10.1103/PhysRevLett.124.187801

Active gels provide a generic and universal model to understand the physics of active materials exerting nonthermal forces on the environment [1,2]. Solutions of biopolymers, such as actin or microtubules, cross-linked by molecular motors, such as myosin or kinesin, are well described by the active gel paradigm [3,4], and so are suspensions of self-motile microorganisms [5,6]. According to the active gel theory, these systems can be modeled as a collection of force dipoles exerted by the active particles (the motors or the microorganisms in the previous examples) on the surrounding fluid [1,2]. Extensile active gels are those in which particles act on the surroundings via outward-pointing dipolar forces; contractile ones exert inward-pointing forces.

Theory [7–14] and experiments [15–17] have shown that active gels possess many intriguing and counterintuitive flow and rheological properties, making them good candidates for new soft functional materials. Extensile fluids flow more easily due to activity, and can behave as "superfluids" with near-zero viscosity [7–11,16,17]. Contractile gels flow instead more *slowly* due to activity [7,10,15]. Theory suggests that the rheology of contractile active gels is reminiscent of that of glasses: These systems should be shear thinning and possess a yield stress when in the nematic phase [12]. While numerical simulations of contractile active gels in the isotropic phase showed that their viscosity tends to infinity as the system approaches the spinodal point [8], whether or not the system should have a yield stress deep in the nematic phase is currently unclear. Here, the complication is that splay fluctuations are known to generically destroy nematic order in a large enough contractile system [18,19], rendering calculations based on spatially homogeneous states inconclusive.

To address the yield stress issue, and to provide a complete theory for active contractile rheology, here we combine computer simulations and analytics to study contractile nematics subjected to a pressure-driven (Poiseuille) flow [Fig. 1(a)]. We define an apparent viscosity, as in experiments, by analyzing the magnitude of the throughput

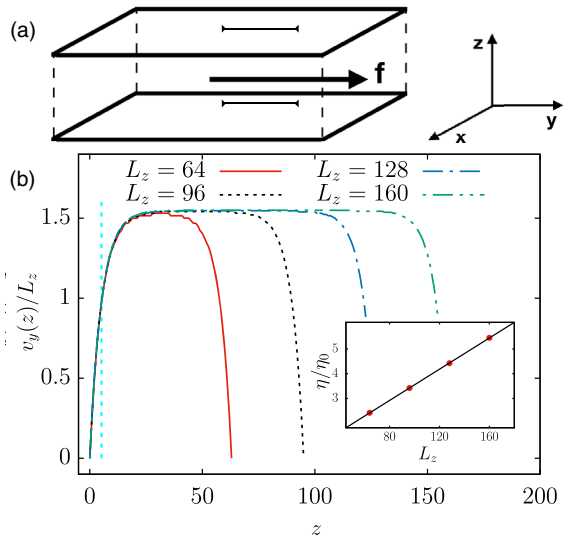

FIG. 1. (a) A schematic diagram of the channel with walls at the boundaries in the z direction and periodic boundaries in x and y. A constant body force $\mathbf{f}$ is applied in the positive y direction. In our quasi-1D geometry Q and $\mathbf{u}$ only depend on z; in 2D simulations, they depend on y and z. (b) Numerical results showing the y component of the velocity (scaled by system size) against z for systems of varying channel width. The permeation length λ_p has been determined by fitting these curves to the velocity field in Eq. (9), thus showing that λ_p (represented by the dotted vertical line) is independent of L_z. The inset shows a plot of η/η_0 in the linear regime of contractile active liquid crystals in one dimension against the channel width L_z.

flow as a function of the forcing. Focusing initially on systems that do not flow spontaneously and on a "quasi-1D" geometry (in which order parameter and flow field vary in only one direction), we find no yield stress behavior, but instead a viscosity which—in the linear regime—increases with sample size. The phenomenology of the associated flow, in particular the flow velocity profile and high apparent viscosity, is strikingly similar to permeation in liquid crystals [20–23] and to Darcy's flow [24], but occurs here in the absence of any substrate friction. Our theory shows that this behavior arises because active forces create a flow opposing that imposed by the pressure gradient, in a way which resembles friction qualitatively resulting in pluglike flow. In 2D or 3D systems, the Darcy-like flow persists only up to a critical length, beyond which we find chaotic behavior, or "active turbulence" [5,6,25–28], with much lower viscosity. Importantly, we find that by changing the flow alignment angle and the amplitude of the nematic order parameter, the range of length scales over which the Darcy-like regime is stable can be increased without bound. This happens in particular when the amplitude of the nematic order parameter approaches zero [29].

To describe the equilibrium behavior of our active nematic fluid, we used a particular Landau–de Gennes free energy $\mathcal{F}$ with density f [30], which has two contributions. The first is a bulk term, which describes the isotropic-nematic transition:

$$f_1 = \frac{A_o}{2}\left(1-\frac{\gamma}{3}\right)Q_{\alpha\beta}^2 - \frac{A_o\gamma}{3}Q_{\alpha\beta}Q_{\beta\gamma}Q_{\gamma\alpha} + \frac{A_o\gamma}{4}(Q_{\alpha\beta}^2)^2. \quad (1)$$

The second term quantifies the cost of elastic distortions in the nematic orientation; in the one elastic constant approximation [31], it reads

$$f_2 = \frac{K}{2}(\partial_\alpha Q_{\beta\gamma})^2. \quad (2)$$

In Eqs. (1) and (2), A_0 is the bulk energy scale, γ is a temperaturelike parameter with an isotropic-to-nematic transition at $\gamma = 2.7$, K is the elastic constant, and $\mathbf{Q}$ is the tensorial order parameter measuring orientational order [31]. We use the repeated index summation convention throughout, with Greek indices denoting Cartesian components.

The equation of motion for $\mathbf{Q}$ is

$$\left(\frac{\partial}{\partial t} + u_\gamma\partial_\gamma\right)Q_{\alpha\beta} - S_{\alpha\beta}(\mathbf{Q},\mathbf{W}) = \Gamma H_{\alpha\beta}, \quad (3)$$

where the first term on the left-hand side describes the advection of rods by a fluid with velocity $\mathbf{u}$. The second term is a tensor that couples the rotation and stretching of the liquid crystals to the flow and has the form

$$\mathbf{S}(\mathbf{Q},\mathbf{W}) = (\xi\mathbf{D}+\mathbf{\Omega})(\mathbf{Q}+\mathbf{I}/3) + (\mathbf{Q}+\mathbf{I}/3)(\xi\mathbf{D}-\mathbf{\Omega}) - 2\xi(\mathbf{Q}+\mathbf{I}/3)\mathrm{Tr}(\mathbf{Q}W), \quad (4)$$

where $\mathbf{D} = (\mathbf{W}+\mathbf{W}^T)/2$ and $\mathbf{\Omega} = (\mathbf{W}-\mathbf{W}^T)/2$ are the symmetric and antisymmetric parts of the velocity gradient tensor $W_{\alpha\beta} = \partial_\beta u_\alpha$, and $\mathbf{I}$ is the identity matrix. The quantity ξ is the flow aligning parameter, which will play an important role in this work. Finally, Γ is the rotational diffusion constant, and the tensor $\mathbf{H}$ is the molecular field, $\mathbf{H} = -\delta\mathcal{F}/\delta\mathbf{Q} + (\mathbf{I}/3)\mathrm{Tr}(\delta\mathcal{F}/\delta\mathbf{Q})$.

The evolution of the fluid velocity field $\mathbf{u}$ is described by the Navier-Stokes equation,

$$\rho(\partial_t + u_\beta\partial_\beta)u_\alpha = f_\alpha + \eta_0\nabla^2 u_\alpha + \partial_\beta\Pi_{\alpha\beta}, \quad (5)$$

where ρ is the fluid density, and f_α is the externally applied pressure gradient. The fluid is assumed to be incompressible. The second term on the right-hand side describes the viscous forces, where η_0 is the background fluid viscosity, and $\Pi_{\alpha\beta}$ is the stress tensor [7,18,25],

$$\Pi_{\alpha\beta} = -P_0\delta_{\alpha\beta} + 2\xi\left(Q_{\alpha\beta}-\frac{1}{3}\delta_{\alpha\beta}\right)Q_{\gamma\mu}H_{\gamma\mu} - \xi H_{\alpha\gamma}\left(Q_{\gamma\beta}+\frac{1}{3}\delta_{\gamma\beta}\right) - \xi\left(Q_{\alpha\gamma}+\frac{1}{3}\delta_{\alpha\gamma}\right)H_{\gamma\beta} - \frac{\partial f}{\partial(\partial_\beta Q_{\gamma\mu})}\partial_\alpha Q_{\gamma\mu} + Q_{\alpha\nu}H_{\nu\beta} - H_{\alpha\nu}Q_{\nu\beta} - \zeta Q_{\alpha\beta}, \quad (6)$$

where the last term is the active stress. The activity ζ is negative for contractile fluids, and positive for extensile systems. For more details, see Ref. [32].

We begin by reporting lattice Boltzmann simulation results for the linear rheology of contractile fluids under Poiseuille flow (Fig. 1; see Ref. [33] for methods). We consider a quasi-1D active nematic (where orientational order and flow velocity only vary along z) confined between two infinite parallel plates at $z = 0$ and $z = L_z$, subject to a constant body force (magnitude f) along y. The nematic order parameter $\mathbf{Q}$ is pinned at the plates to $\mathbf{Q}_0 = q(\hat{\mathbf{y}}\hat{\mathbf{y}} - \mathbf{I}/3)$, where the magnitude q of the order parameter is determined by minimizing the bulk free-energy density in Eq. (1), which gives $q = \frac{1}{4}(1+\sqrt{9-24/\gamma})$. We also impose no-slip boundary conditions $\mathbf{u} = \mathbf{0}$ at the plates.

We define an apparent viscosity $\eta = \eta_0 M_0/M$ in terms of the throughput flow of the active nematic, with $M = \int_0^{L_z} dz v_y(z)$, and M_0 the value for a Newtonian fluid with viscosity η_0 in a channel of the same width and subject to the same body force. The velocity profiles in the steady state are shown in Fig. 1(b) for different values of system size L_z (and the same value of f). These correspond to the linear regime, so that further decreasing f leads to no changes in η. We find no sign of a yield stress. Notably, though, we find pluglike flow for all L_z, with near-uniform

velocity in the bulk of the channel, and all the shear confined in a small region close to the wall [Fig. 1(b)]. An analysis of the profiles in Fig. 1(b) shows that the maximum velocity scales as L_z, whereas the length scale over which v_y drops to 0 (the "permeation length" λ_p) does not vary appreciably with size.

To better understand these results, we linearize the steady state equations of motion for our quasi-1D case to obtain

$$\Gamma K \delta Q'' + x_2 v' = 0,$$
$$\eta_0 v'' - \zeta \delta Q' - x_2 K \delta Q''' + f = 0, \tag{7}$$

where $x_2 \equiv [2\xi + q(\xi - 3)]/6$ [33], whereas $\delta Q = \delta Q_{yz}$ and $v = u_y$ are the deviations of the order parameter tensor and the flow field from their rest values ($\mathbf{Q} = \mathbf{Q}_0$ and $\mathbf{u} = \mathbf{0}$) due to the body force f. This set of equations—which is a valid approximation of the full model in the linear regime of $f \to 0$—is solved by

$$\delta Q = \frac{f L_z}{2|\zeta|}\left(\frac{\sinh(\delta z/\lambda_p)}{\sinh(L_z/2\lambda_p)} - \frac{2\delta z}{L_z}\right), \tag{8}$$

$$v = \frac{K\Gamma f L_z \coth(L_z/2\lambda_p)}{2x_2\lambda_p|\zeta|}\left[1 - \frac{\cosh(\delta z/\lambda_p)}{\cosh(L_z/2\lambda_p)}\right] \tag{9}$$

with $\delta z = z - L_z/2$. The flow field in Eq. (9) corresponds to pluglike flow [Fig. 1(b)], with constant velocity except in a boundary layer of size $\lambda_p = \sqrt{[(\Gamma\eta_0 K + 2Kx_2^2)/(|\zeta|x_2)]}$. For sufficiently large $\Gamma\eta_0$, the permeation length $\lambda_p \sim l_a\sqrt{\Gamma\eta_0}$, where we have introduced the active length scale $l_a = \sqrt{K/|\zeta|}$. This scaling holds in our simulations (Fig. S1 in the Supplemental Material [33]).

Integrating the velocity over the channel, we obtain $M = \int_0^{L_z} v dz$. This leads to

$$\eta = \frac{L_z\lambda_p x_2|\zeta|}{6\Gamma K[\coth(\frac{L_z}{2\lambda_p}) - 2\frac{\lambda_p}{L_z}]}. \tag{10}$$

The apparent viscosity η tends to a constant for $L_z \ll \lambda_p$, and increases linearly with L_z for $L_z \gg \lambda_p$, as found numerically [Fig. 1(b), inset]. Our theory shows that the nontrivial behavior is due to the pluglike flow velocity profile, which occurs here *despite* the absence of a frictional substrate. This is reminiscent of Darcy's flow in porous media [24], or of permeative flows in cholesteric liquid crystals [22,23]. We therefore refer to this linear regime of contractile fluids as the "Darcy" regime. A Darcy-like flow appears because Eq. (7) implies that $\delta Q'' \propto v'$ in steady state, so that the terms dependent on $\delta Q'$ in Eq. (8) introduce, among others, a term linear in v, which is formally similar to the contribution describing friction with a substrate. Physically, the mechanism underlying the onset of a Darcy-like pluglike flow is that the active flow due to the nontrivial order parameter profile pulls back on the fluid and opposes the externally imposed flow. This results in the removal of gradients of the order parameter and the velocity in the bulk.

To address the stability of the Darcy regime as a function of the pressure gradient, we now study the nonlinear rheology of active contractile nematics. Inspection of Eq. (5) suggests that in steady state we may expect a balance between the body force and the divergence of the stress tensor. The latter should be dominated by the active contribution $\sim|\zeta|$ [7]. Dimensional analysis then yields $\tilde{f} = fl/|\zeta|$ as a potential control parameter, which determines the relative weight between external forcing and internal active stresses; we call this an active Ericksen number. Here, l is a length quantifying the scale over which the active stress and orientation order vary spatially; in our simulations, we find the relevant length scale to be L_z, hence, $\tilde{f} = fL_z/|\zeta|$.

Figure 2 plots the apparent viscosity found in simulations as a function of $\tilde{f}$. We find that all the curves collapse for sufficiently large values of $\tilde{f}$, whereas they diverge for small forcing (to yield the linear regime apparent viscosity discussed in Fig. 1). In other words, there is a crossover between the Darcy regime and a universal shear thinning regime, which is singly determined by $\tilde{f}$. The dependence of the apparent viscosity on $\tilde{f}$ can be understood via a qualitative scaling argument which adds the Newtonian and the opposing active contribution to the throughput flow M, as shown in [33].

The quasi-1D approximation described above is useful, as it allows a complete characterization of the rheology of a contractile gel, together with an analytically tractable theory which uncovers the mechanism leading to a Darcy-like linear regime with no yield stress. However,

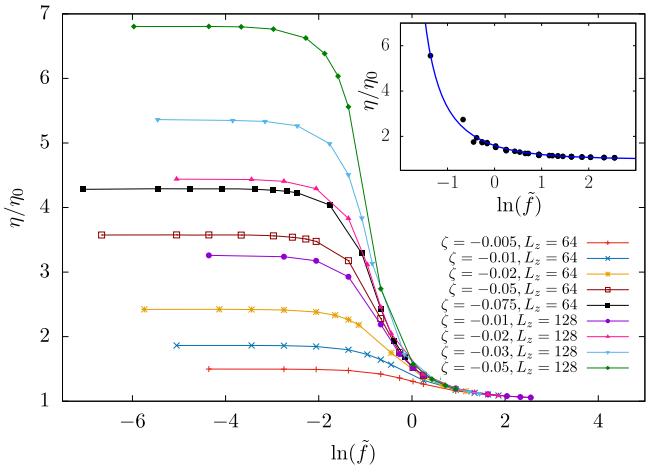

FIG. 2. Plot of η/η_0 against $\ln(\tilde{f})$ from numerical simulation of a quasi-1D contractile active material. At lower $\tilde{f}$, η/η_0 is constant and increases with the channel width. The inset shows a fit to $[(1 + b\tilde{f})/(b\tilde{f} - c)]$, with b, $c > 0$.

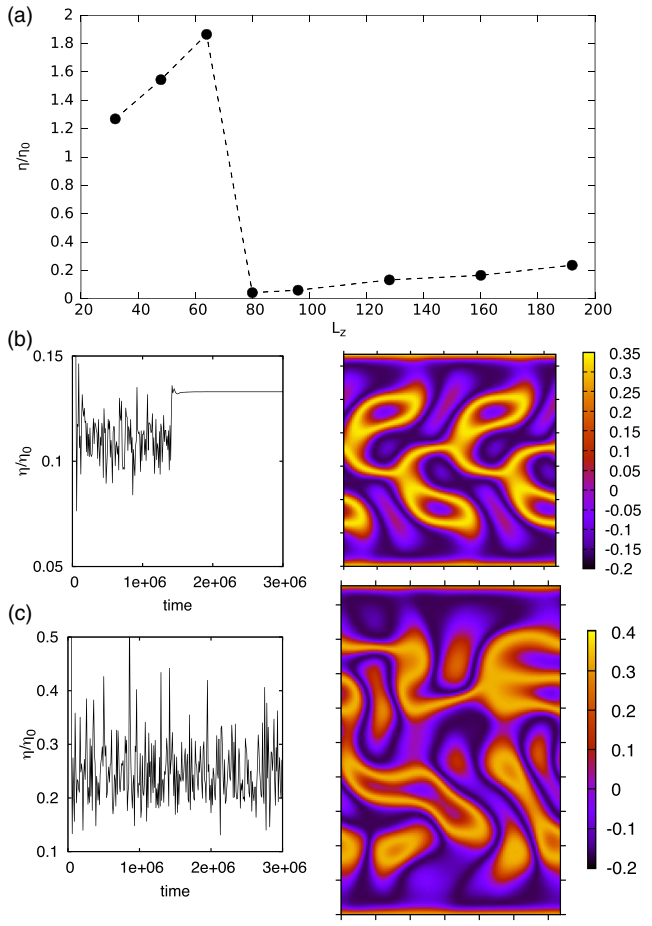

FIG. 3. (a) A plot of η/η_0 against L_z for small fixed body force ($f = 10^{-6}$) for contractile active nematics ($|\zeta| = 0.01$). (b) Viscosity versus time (left) and Q_{yz} pattern (right) for a system with $L_z = 128$. (c) Viscosity versus time (left) and Q_{yz} pattern for a system with $L_z = 192$. Axes tics in the right patterns in (b),(c) are shown every 20 lattice sites.

the persistence of the Darcy regime to arbitrarily large system size, which we observe in Fig. 1, is due to the special features of our effectively 1D geometry [25,37]. In a fully 2D or 3D system, we only expect the Darcy regime to be stable up to a finite system size, as it has long been known [18] that infinitesimal splay fluctuations destabilize the uniform state of the contractile active nematic for $L_z > L_c$—an instability length scale proportional to l_a.

To explore the more general problem of 2D contractile rheology, we now use simulations to study the case in which the $\mathbf{Q}$ tensor and velocity fields depend on both y and z [though orientational order and flow can also point out of the (y, z) plane] [38]. We focus on the case of a fixed (small) value of f. Figure 3(a) shows η as a function of system size L_z. As anticipated, the Darcy-like regime (corresponding to the increase of η with L_z) gives way to another regime—characterized by much smaller viscosity—beyond the instability length scale L_c.

In the unstable regime, the apparent viscosity varies chaotically over time, so that the system is in the active turbulent regime, best characterized for extensile fluids [5]. Remarkably, we find that in several cases the chaotic dynamics settles into a spatially dependent nontrivial traveling wave pattern; an example of the resulting $\mathbf{Q}$ tensor texture is shown in Fig. 3(b). The existence of multiple possible nontrivial traveling wave solutions is reminiscent of the phenomenology of low-dimensional models for Newtonian turbulence [39], although here these states appear to be linearly stable. The traveling wave states and turbulent patterns both involve a characteristic length scale, which in our simulations is close to the active length scale l_a known to set the typical vortex size in active turbulence [32]. For sufficiently large $\tilde{f}$, we reenter the 1D shear thinning pattern, as the forcing is strong enough to suppress variation along the flow direction (as for shear [40]; Fig. S2 in the Supplemental Material [33]).

To complement our simulations, we calculated exactly the value of L_c—beyond which the Darcy regime is unstable in 2D [38] with our boundary conditions—by using a spectral Chebyshev method [33,41]. Figure 4 plots the dependence of L_c on ξ, and shows that increasing the flow aligning parameter leads to a dramatic enhancement of the stability range of the quasi-1D Darcy regime. By following Ref. [42], we can relate ξ to microscopic parameters accessible experimentally via the formula

$$\xi = \frac{2\frac{I_L+2I_s}{I_L-I_s}+q}{2+q}, \tag{11}$$

where I_L and I_s are, respectively, the largest eigenvalue of the moment of inertia tensor of the constituent nematogens, and the mean of the two smallest eigenvalues.

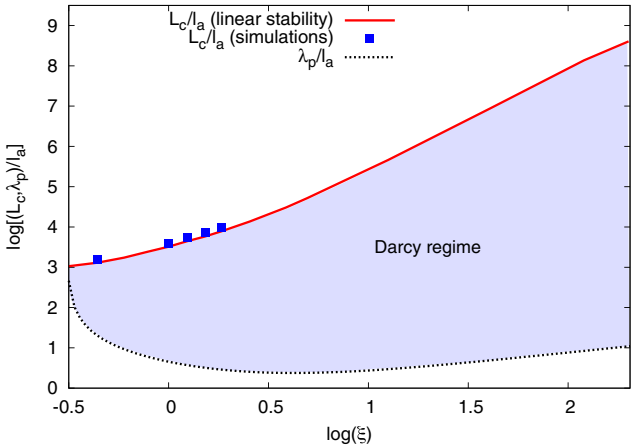

FIG. 4. Log-log plot of the instability length scale L_c (solid line, exact numerics, and filled squares, lattice Boltzmann) and of λ_p (dotted line) as a function of ξ, for $A_0 = 1$, $\gamma = 3$, $q = 1/2$, $\Gamma = 0.33775$, $\eta_0 = 5/3$, $K = 0.04$, and variable ζ. Length scales are in units of l_a.

Equation (11) and Fig. 4 predict that, for instance, $I_L/I_s = 4$ and $q = 1/2$ give $\xi = 1.8$, for which $L_c/\lambda_p \simeq 60$ (Fig. 4), corresponding to a large Darcy regime.

Another way to increase the stability range of the Darcy regime is to decrease the value of the nematic order $q \to 0$ [33]. This limit could be reached in models in which the cubic term in Eq. (1) gets very small (for instance, a theory for weakly ordered thin actomyosin films), or in mixtures of prolate and oblate molecules [29].

In summary, we have shown that an active contractile nematic subjected to a pressure-driven flow does not possess a yield stress, and evades it by instead acquiring a size-dependent viscosity associated with pluglike flow which is reminiscent of Darcy's flow in porous materials. The Darcy regime is always found in a quasi-1D geometry (with variation of order and flow along a single direction) for sufficiently small values of the body force. In a 2D geometry, the Darcy regime is instead only observed up to a critical system size, beyond which we have found chaos and active turbulence. The range of stability of the Darcy regime in 2D is tunable, and can be increased virtually indefinitely by a suitable choice of parameters. In particular, our results have suggested that this range can be very large in thin and weakly ordered films of actomyosin, for which l_a is a few microns [43]. We hope this prediction will stimulate experiments on channel flow in active contractile systems—such as, but not limited to, myosin-filament mixtures—aimed at observing all rheological regimes we predict here—Darcy flow, shear thinning. and chaos.

We thank the Higgs Centre for Theoretical Physics for supporting two of J. T.'s visits to the University of Edinburgh, during which part of this work was performed.

[1] S. Ramaswamy, Annu. Rev. Condens. Matter Phys. **1**, 323 (2010).
[2] M. C. Marchetti, J.-F. Joanny, S. Ramaswamy, T. B. Liverpool, J. Prost, M. Rao, and R. A. Simha, Rev. Mod. Phys. **85**, 1143 (2013).
[3] T. Sanchez, D. T. N. Chen, S. J. DeCamp, M. Heymann, and Z. Dogic, Nature (London) **491**, 431 (2012).
[4] M. S. e Silva, M. Depken, B. Stuhrmann, M. Korsten, F. C. MacKintosh, and G. H. Koenderink, Proc. Natl. Acad. Sci. U.S.A. **108**, 9408 (2011).
[5] H. H. Wensink, J. Dunkel, S. Heidenreich, K. Drescher, R. E. Goldstein, H. Löwen, and J. M. Yeomans, Proc. Natl. Acad. Sci. U.S.A. **109**, 14308 (2012).
[6] A. Sokolov, I. S. Aranson, J. O. Kessler, and R. E. Goldstein, Phys. Rev. Lett. **98**, 158102 (2007).
[7] Y. Hatwalne, S. Ramaswamy, M. Rao, and R. A. Simha, Phys. Rev. Lett. **92**, 118101 (2004).
[8] M. E. Cates, S. M. Fielding, D. Marenduzzo, E. Orlandini, and J. M. Yeomans, Phys. Rev. Lett. **101**, 068102 (2008).
[9] L. Giomi, T. B. Liverpool, and M. C. Marchetti, Phys. Rev. E **81**, 051908 (2010).
[10] D. Saintillan, Annu. Rev. Fluid Mech. **50**, 563 (2018).
[11] A. Loisy, J. Eggers, and T. B. Liverpool, Phys. Rev. Lett. **121**, 018001 (2018).
[12] T. B. Liverpool and M. C. Marchetti, Phys. Rev. Lett. **97**, 268101 (2006).
[13] D. Marenduzzo, E. Orlandini, and J. M. Yeomans, Phys. Rev. Lett. **98**, 118102 (2007).
[14] S. M. Fielding, D. Marenduzzo, and M. E. Cates, Phys. Rev. E **83**, 041910 (2011).
[15] S. Rafaï, L. Jibuti, and P. Peyla, Phys. Rev. Lett. **104**, 098102 (2010).
[16] H. M. López, J. Gachelin, C. Douarche, H. Auradou, and E. Clément, Phys. Rev. Lett. **115**, 028301 (2015).
[17] V. A. Martinez *et al.*, Proc. Natl. Acad. Sci. U.S.A. **117**, 2326 (2020).
[18] R. A. Simha and S. Ramaswamy, Phys. Rev. Lett. **89**, 058101 (2002).
[19] S. Ramaswamy and M. Rao, New J. Phys. **9**, 423 (2007).
[20] W. Helfrich, Phys. Rev. Lett. **23**, 372 (1969).
[21] P. M. Chaikin and T. C. Lubensky, *Introduction to Condensed Matter Physics* (Cambridge University Press, Cambridge, England, 1995).
[22] D. Marenduzzo, E. Orlandini, and J. M. Yeomans, Phys. Rev. Lett. **92**, 188301 (2004).
[23] D. Marenduzzo, E. Orlandini, and J. M. Yeomans, J. Chem. Phys. **124**, 204906 (2006).
[24] S. Whitaker, Transport Porous Med. **1**, 3 (1986).
[25] D. Marenduzzo, E. Orlandini, M. E. Cates, and J. M. Yeomans, Phys. Rev. E **76**, 031921 (2007).
[26] S. P. Thampi, R. Golestanian, and J. M. Yeomans, Phys. Rev. Lett. **111**, 118101 (2013).
[27] C. Dombrowski, L. Cisneros, S. Chatkaew, R. E. Goldstein, and J. O. Kessler, Phys. Rev. Lett. **93**, 098103 (2004).
[28] A. Sokolov and I. S. Aranson, Phys. Rev. Lett. **109**, 248109 (2012).
[29] Since the isotropic-nematic transition is first order, there is usually a lower bound on the amplitude of q. However, as one approaches a prolate-oblate-biaxial nematic multicritical point [see R. Alben, Phys. Rev. Lett. **30**, 778 (1973)], the size of the first order jump vanishes. Hence, near such a multicritical point, which can be realized experimentally by mixing prolate and oblate molecules, it is possible to make the nematic order parameter arbitrarily small.
[30] A. N. Beris and B. J. Edwards, *Thermodynamics of Flowing Systems: With Internal Microstructure* (Oxford University, New York, 1994).
[31] P. D. deGennes and J. Prost, *The Physics of Liquid Crystals* (Clarendon Press, Oxford, 1993).
[32] A. Doostmohammadi, J. Ignés-Mullol, J. M. Yeomans, and F. Sagués, Nat. Commun. **9**, 3246 (2018).
[33] See Supplemental Material at http://link.aps.org/supplemental/10.1103/PhysRevLett.124.187801 for details of our numerical scheme, additional results, and a description of the exact numerics used to obtain the results in Fig. 4. Also included in the Supplemental Material Refs. [34–36].
[34] C. Denniston, E. Orlandini, and J. M. Yeomans, Phys. Rev. E **63**, 056702 (2001).
[35] A. Morozov and W. van Saarloos, J. Stat. Phys. **175**, 554 (2019).
[36] E. Jones, T. Oliphant, P. Peterson *et al.*, SciPy: Open source scientific tools for PYTHON, https://www.scipy.org/, 2001.

[37] S. A. Edwards and J. M. Yeomans, Europhys. Lett. **85**, 18008 (2009).
[38] Selected 3D lattice Boltzmann simulations suggest that L_c is the same in 2D and 3D.
[39] F. Waleffe, Phys. Fluids **9**, 883 (1997).
[40] S. Muhuri, M. Rao, and S. Ramaswamy, Europhys. Lett. **78**, 48002 (2007).
[41] C. Canuto, M. Hussaini, A. Quarteroni, and T. Zang, *Spectral Methods in Fluid Dynamics* (Springer, Berlin, 1988).
[42] D. Forster, Phys. Rev. Lett. **32**, 1161 (1974).
[43] M. Nishikawa, S. R. Naganathan, and F. Julicher, eLife **6**, e19595 (2017).